

Physical pendulum model: Fractional differential equation and memory effects

L. N. Gonçalves,^{1,2,*} J. Fernandes,³ A. Ferraz,^{3,2} A. G. Silva,^{1,4} and P. J. Sebastião^{3,2}

¹*Departamento de Física, Faculdade de Ciências e Tecnologia, Universidade Nova de Lisboa, 2829-516 Caparica, Portugal*

²*CeFEMA, Av. Rovisco Pais, 1, 1049-001 Lisboa, Portugal*

³*Departamento de Física, Instituto Superior Técnico, Universidade de Lisboa, Av. Rovisco Pais, 1, 1049-001 Lisboa, Portugal*

⁴*CeFiTec, Faculdade de Ciências e Tecnologia, Universidade Nova de Lisboa, 2829-516 Caparica, Portugal*

(Dated: June 13, 2022)

A detailed analysis of three pendular motion models is presented. Inertial effects, self-oscillation, and memory, together with non-constant moment of inertia, hysteresis and negative damping are shown to be required for the comprehensive description of the free pendulum oscillatory regime. The effects of very high initial amplitudes, friction in the roller bearing axle, drag, and pendulum geometry are also analysed and discussed. The model that consists of a fractional differential equation provides both the best explanation of, and the best fits to, experimental high resolution and long-time data gathered from standard action-camera videos.

This article has been published by
American Journal of Physics
at <https://doi.org/10.1119/10.0001660>

I. INTRODUCTION

There's no classic like the physical pendulum. It has been the subject of scientific enquiry since Galileo first observed its isochrony [1]. It has been a source of technological development since Huygens' pendulum clock [2]. It has been a reference instrument since at least 1818 [3–5] and it plays a fundamental role in the implementation of gravitational wave observatories [6–9]. To this day, the pendulum continues to serve as a tool to understand many diverse phenomena involving both oscillation and relaxation [10] like parametric pumping (e.g. pendulum clock, swing, roller skating) [11–14], hysteresis [15, 16], deterministic chaos [17, 18], charge density waves [19, 20], “macroscopic quantization” [21–24], bosonic Josephson junctions [25], classical micro-canonical systems [26, 27] and dielectric relaxation [28–31]. The physical pendulum may even contribute to the understanding of some climate change effects like meteotsunamis [32].

The theoretical description of pendular motion has been the subject of many studies, some of which gave rise to very sophisticated equations of motion [33–37]. However, one that accurately matches long-time data, of a very high amplitude physical pendulum, has been lacking. This probably stems from lacking observations of the hysteretic nature of pendular motion. This observation is now made and justifies the proposed fractional model. This model fits experimental data gathered with a modern action-camera and explains the observed hysteresis on the basis of memory, non-constant moment of inertia and self-oscillation.

Modern studies of the interdependency of amplitude on the period seem to have started on the seventies of

the XXth century [38, 39]. Fourier transform analysis was used to advance those studies [40, 41]. A tentatively realistic model of the pendulum motion, considering constant, linear and quadratic drag terms, was introduced by Squire [42] and studied in diverse combinations [43–49]. More recently, Mathai *et al.* proposed a dry-friction damping term dependent on the pendulum angle when studying an underwater pendulum [50]. The study of underwater pendula make apparent the effects of the surrounding fluid [50–52]. In particular the emission of vortex rings at extreme angles was put in evidence by Bolster *et al.* [52].

Other experiments that provide insight into pendular motion include the air-track [53, 54], the drinking straw [55, 56], and the free-fall [57].

From the experimental point of view the study of pendular motion can be conducted by measuring the angular position of the moving object or by measuring its acceleration. Recently, different studies used the latter approach [35, 54, 58, 59].

It is worth mentioning that the study of pendular motion is a subject in the extensive area of parameter identification of vibrating systems [60, 61].

This paper is organized as follows. The experimental setup is presented in section II together with some contextualizing data. The theoretical analysis regarding the equation of motion, is introduced in section III. Two initial conceptual models are presented and tested in sections IV and V. An introduction to time fractional derivatives and the concept of memory follows. We move on describing the fractional differential equation of motion and associated results. We finish with a general conclusion.

II. EXPERIMENTAL

The physical pendulum used in this work is composed of: a 2.5 cm diameter roller bearing concentric with an hollow acrylic disc with a diameter of 6 cm; a 52 cm long squared cross-section hollow bar; and a slightly longer threaded steel 6 mm thick rod that is screwed both to

* lng@fct.unl.pt

TABLE I. Run code infixes (e.g. `##1a#` as explained in the text).

	with alley	without alley
launched	la	ln
not launched	na	nn

the square bar and to the acrylic hollow disc by two nuts. Rectangular tiles, 18 cm wide and with lengths $l_1 = (3 \times n)$ cm where $n = 1, \dots, 8$, made of cardboard, foam and tape were fixed at the end of the square bar. Three slabs of composite cardboard, assembled to form an alley, were used in half the measurement runs.

Figure 1 shows schematics of the apparatus. Videos were recorded with a Sony HDR-AS100V action-camera using a resolution of 1280x720 pixels at 120 frames per second (FPS). The camera was placed directly in front and aligned with the pendulum axle at a distance of approximately 58 cm. In this way the tracking spot was always within the maximum possible camera view field. A pink[63] circular tracking spot was glued to the pendulum at approximately 26 cm from the axle and facing the camera lens (see Figure 1). This tracking spot orientation made possible to obtain a permanent circular tracking template that contributed to avoid rotation artifacts. A careful illumination of the apparatus proved necessary to minimize motion blur.

The experimental $\theta(t)$ data was collected using the open source video analysis tool Tracker [64]. The radial distortion of the video frames was corrected using the “Fisheye” filter at 120° and 48% fixed pixels. The tracking algorithm compares, for each frame, a previously defined mark template with the current image within the tracking target area. In view of the large number of video frames that are tracked on a single video (may be larger than 10^4), the Tracker’s “evolution rate” was set at 0%. Also, due to heterogeneous lighting, the Tracker’s “automark” was reduced to 3 to obtain a manageable rejection rate.

A sequence of experimental runs was conducted according to the following procedure. In each run the pendular motion was recorded from an initial launch to its stopping. Four kinds of measurement runs were analysed: launched (1) with initial speed; released from rest; with alley (a); and without alley. In Table I the two letters codes used to identify each kind of run are presented. For each kind of run two additional digits identify the tile length: no tile (00); 3 cm long tile (03); 6 cm long tile (06), etc. up to 24 cm long tile (24) in steps of 3 cm. The complete run codes include also an end digit identifying the trial number of each run kind. For example, `06na5` refers to the fifth run using the 6 cm long tile without launch but with alley.

In all runs the zero angle was defined by the pendulum’s final stopping position, the initial angle was always $\theta_{\text{ini}} \geq \pi$ rad and the initial angular velocity was always $\omega_{\text{ini}} \leq 0$.

Each run has its own specificity. The video camera

position and orientation affect pendulum angle measurement. The position and orientation of the lamps may produce reflections that affect some of the video-frames. The final equilibrium position may not be exactly vertical. The roller bearing has some clearance and allows sideways oscillations that may affect the main oscillation. When a tile enters or exits the alley its motion may be subject to sudden perturbations. These specificities, while unavoidably present, do not seem to significantly affect the experimental data.

Some exploratory $\theta(t)$ runs are presented In Figure 2 to illustrate how the pendular motion depends on different initial conditions. The angular acceleration $\alpha = \frac{d^2\theta}{dt^2}$ is plotted in Figure 3 as a function of the extreme angles θ_{ext} (for which the angular velocity $\omega = \frac{d\theta}{dt}$ is zero). The values of both ω and α are obtained directly from $\theta(t)$ data via Savitzky-Golay filters [65] using cubic polynomials and windows of 25 points (25 consecutive video frames). It is clear that $\alpha(\theta_{\text{ext}})$ is well fitted by a sine function with a coefficient of proportionality $-\Omega_0^2$:

$$\alpha(\omega = 0) \approx -\Omega_0^2 \sin \theta_{\text{ext}}. \quad (1)$$

The acceleration may be evaluated relatively to this function for any velocity:

$$\Delta\alpha(\omega) = \alpha(\omega) + \Omega_0^2 \sin \theta(\omega). \quad (2)$$

This is plotted in Figure 4 which puts in evidence the hysteric nature of pendular motion. Note that Figures 3 and 4 constitute mappings of the three-dimensional data plotted in Figure 18.

III. GENERAL EQUATION OF MOTION

The net torque \mathcal{T}_{net} acting on the pendulum is

$$\mathcal{T}_{\text{net}} = \frac{dL}{dt} = \frac{dI}{dt}\omega + I\alpha \quad (3)$$

where $L = I\omega$ is the angular momentum, t is time, I is the moment of inertia, $\omega = \frac{d\theta}{dt}$ is the angular velocity, and $\alpha = \frac{d\omega}{dt}$ is the angular acceleration. Under the assumption of uniform air density and negligible pressure gradients, the net torque is also the sum of gravitic and dissipative torques $\mathcal{T}_{\text{net}} = \mathcal{T}_{\text{grav}} + \mathcal{T}_{\text{diss}}$, so

$$I\alpha = \mathcal{T}_{\text{grav}} + \mathcal{T}_{\text{diss}} - \frac{dI}{dt}\omega. \quad (4)$$

Usually, it is assumed that the pendulum is a strictly rigid body, its moment of inertia is therefore constant and the $-\frac{dI}{dt}\omega$ term vanishes. However, we may assume this term to be neither conservative nor dissipative

$$-\frac{dI}{dt}\omega = \mathcal{T}_{\text{iner}} \quad (5)$$

but inertial and dependent on the air surrounding the pendulum as noted by Squire [42]:

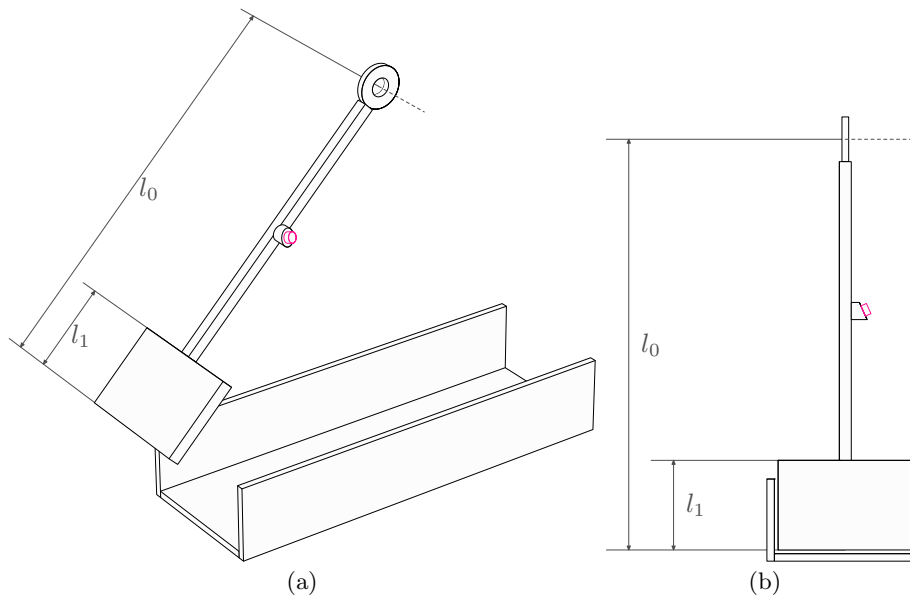


FIG. 1. Schematics [62] of the apparatus: (a) perspective view with $\theta = \pi/4$ rad; (b) orthogonal view with $\theta = 0$. There may be a tile with an edge at the pendulum extreme (at a distance l_0 from the axle) and another edge at a distance $l_0 - l_1$ (the height of the tile is l_1). Also, there may be an alley for the pendulum to pass through without touching. There is a clearance of approximately half centimeter between the pendulum and the alley. The schematics are drawn to scale showing both the pink tracking spot and a $l_1 = 12$ cm tile.

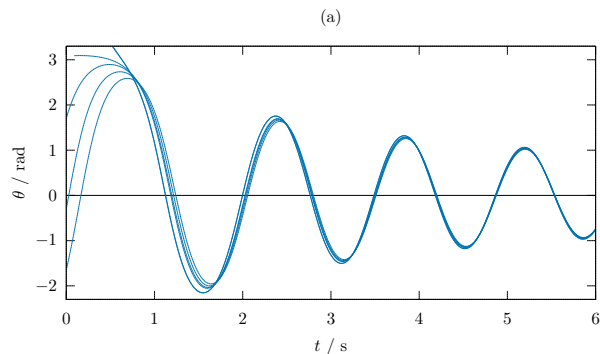


FIG. 2. Superposition of five exploratory runs made with a $l_1 = 12$ cm tile, without alley and different initial conditions. One of the runs starts from rest at an initial angle close to π rad. For each run a time shift was introduced to allow a superposition of all runs at $t = 10$ s.

What does seem clear is that the acceleration of an oscillating body causes acceleration in the entrained air around it [...].

From this point of view it is reasonable to expect that the inertia does not change significantly when either the pendulum is not moving ($\omega = 0$) or its velocity is not changing ($\alpha = 0$). On the contrary, we expect inertia to change when velocity is changing ($\alpha \neq 0$). Furthermore, the greater the velocity, the greater the amount of displaced air per unit time. Therefore, the changes of inertia may be considered proportional to velocity, as a first approximation. There is also the possibility that

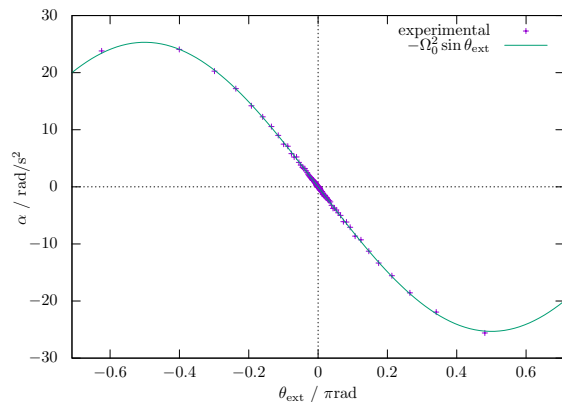


FIG. 3. Initial analysis of acceleration and angle for run 241a1 (see text).

the amount of air in coherent motion with the pendulum may be directly correlated with the moment of inertia. In this way the changes of inertia may be considered proportional to acceleration, velocity, and moment of inertia:

$$\frac{dI}{dt} = \tau^2 I \omega \alpha \quad (6)$$

where τ is an inertial characteristic time. A dimensional analysis of the above expression provides some additional insight on the underlying physics of this phenomenon. In fact, $I\omega\alpha$ has dimensions of power, therefore, equation (6) states that the rate of change of I is proportional to a power and is positive when ω and α have the same

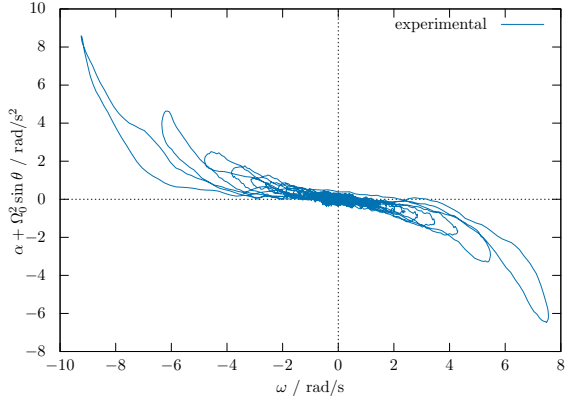


FIG. 4. Initial analysis of experimental data for run 241a1 (see text).

sign. Also, it is worth to note that $\tau^2 I \omega \alpha$ has dimensions of $ML^2T^{-1} = (ML^{-1}T^{-1})L^3$, which is viscosity times volume. In this way, the same rate of change of inertia can be obtained either with low viscosity and big volume or with high viscosity and small volume.

The integration of equation (6) is straightforward and provides

$$I = I_0 e^{\frac{(\tau\omega)^2}{2}} \quad (7)$$

where I_0 is the moment of inertia at rest, leading to

$$L = I_0 \omega e^{\frac{(\tau\omega)^2}{2}}. \quad (8)$$

As a consequence of this, L depends not only on $I_0 \omega$ but also on a speed dependent factor that “inflates” the angular momentum.

Inserting equation (6) in equation (5), one finds

$$\mathcal{T}_{\text{iner}} = -I(\tau\omega)^2 \alpha \quad (9)$$

and inserting equation (6) in equation (4), the result is

$$\alpha = \frac{\mathcal{T}_{\text{grav}}}{I} + \frac{\mathcal{T}_{\text{diss}}}{I} - (\tau\omega)^2 \alpha \quad (10)$$

where the term $-(\tau\omega)^2 \alpha$ was already found by Basano *et al.* [57].

In conclusion

$$\alpha = \frac{\mathcal{T}_{\text{grav}} + \mathcal{T}_{\text{diss}}}{(1 + \omega^2 \tau^2) I} \quad (11)$$

meaning that the pendulum is no longer considered a strictly rigid body because of the changing amount of air that is dragged along and moves coherently with the rigid pendulum. It is interesting to note that similar phenomena has been observed with water column oscillators [55, 56].

The gravitic torque can be expressed as

$$\mathcal{T}_{\text{grav}} = -Mgl_{\text{com}} \sin \theta \quad (12)$$

where M is the effective gravitic mass of the pendulum (discounting buoyancy) and l_{com} is the distance between the rotation axle and the center of mass (see Figure 1). It is important to note that the air surrounding the pendulum contributes to inertia, equation (6), but neither contributes to gravitic mass nor to the center of mass because it has null effective mass.

Inserting equation (12) and equation (7) in equation (11) we obtain

$$\alpha = \frac{\frac{\mathcal{T}_{\text{diss}}}{I_0} - \Omega_0^2 \sin \theta}{(1 + \omega^2 \tau^2) e^{\frac{(\tau\omega)^2}{2}}}. \quad (13)$$

where

$$\Omega_0 = \sqrt{\frac{Mgl_{\text{com}}}{I_0}} \quad (14)$$

is, by definition, the natural angular frequency.

As shall be confirmed in Figure 7, the denominator in equation (13) may be twice linearized in $x = (\tau\omega)^2$:

$$\frac{1}{(1 + (\tau\omega)^2) e^{\frac{(\tau\omega)^2}{2}}} \approx \frac{1}{1 + \frac{3}{2}(\tau\omega)^2} \approx 1 - \frac{3}{2}(\tau\omega)^2 \quad (15)$$

Equation (13) can, then, be written as a general equation of motion:

$$\alpha + \Omega_0^2 \sin \theta = \alpha_{\text{diss}} + \alpha_{\text{iner}} \quad (16)$$

in terms of both

$$\alpha_{\text{diss}} = \frac{\mathcal{T}_{\text{diss}}}{I_0} \left(1 - \frac{3}{2}(\tau\omega)^2\right) \quad (17)$$

and

$$\alpha_{\text{iner}} = \frac{3}{2}(\tau\omega\Omega_0)^2 \sin \theta = C_a \omega^2 \sin \theta, \quad (18)$$

where $C_a = \frac{3}{2}(\tau\Omega_0)^2$ is a non-dimensional coefficient that measures the effect of “added mass” [66–71]. Equation (18) is similar to the inertial nonlinearity term introduced by Kavyanpoor and Shokrollahi [36] in a generalized Duffing oscillator equation of motion. Suppose now that $\alpha_{\text{diss}} = 0$ in equation (16). Then we have

$$\alpha + (\Omega_0^2 - C_a \omega^2) \sin \theta = 0. \quad (19)$$

Note that the “added mass” reduces the angular frequency of the pendulum. This reduction may be named “inertial redshift” in analogy with what is known as “damping redshift” [72]. Equation (19) provides the following solution for a pendulum that initiates its movement from rest at an angle θ_0 .

$$\frac{\omega}{\Omega_0} = \sqrt{\frac{1 - e^{2(\cos \theta_0 - \cos \theta)} C_a}{C_a}} \quad (20)$$

This solution is plotted in Figure 5 and proves that $\mathcal{T}_{\text{iner}}$ in fact is not dissipative because the solution is an even

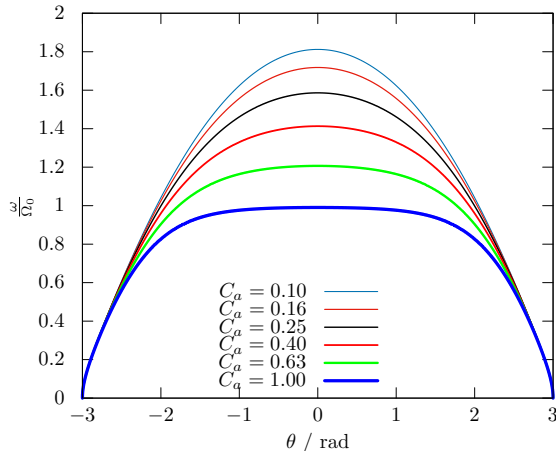


FIG. 5. Plots of equation (20) with $\theta_0 = -3$ rad.

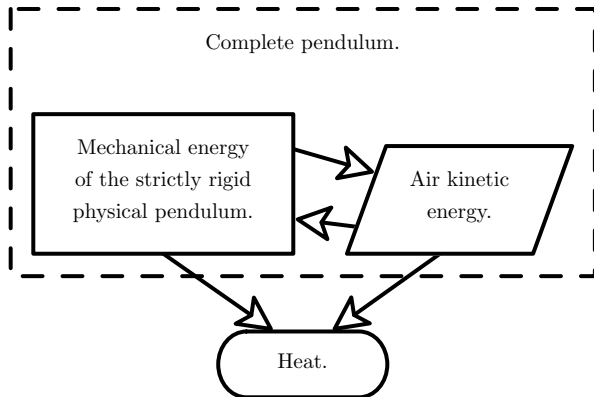


FIG. 6. Schematics of the energy exchanges taking place during the physical pendulum motion. Part of the mechanical energy of the pendulum is converted into kinetic energy of the air. Some of this kinetic energy is recovered. The remaining part is dissipated as heat.

function in θ (the speed returns to the same value after a full swing). Figure 5 reflects the effect of equation (6): when the speed is increasing the moment of inertia is also increasing. The very curious consequence of this moment of inertia evolution is that when the speed increases, the ratio acceleration to velocity shows a flattening behaviour. In fact, this is equivalent: (i) to a storage of kinetic energy in the air when the speed is increasing; and (ii) to a release of kinetic energy from the air to the strictly rigid part of the pendulum when the speed is decreasing. This stored kinetic energy is converted into potential energy because the air that moves together with the strictly rigid part of the pendulum provides a “gentle push”. This “gentle push” constitutes a kind of parametric pumping [11, 12]. Figure 6 contains a schematic diagram of the energy exchanges taking place.

A. Mechanical energy

In order to calculate the mechanical energy, we start by rewriting equation (13) with the first linearization of equation (15) in the form of a specific torques equation as follows:

$$\left(1 + \frac{3}{2}(\tau\omega)^2\right)\alpha + \Omega_0^2 \sin\theta = \frac{\mathcal{T}_{\text{diss}}}{I_0}. \quad (21)$$

On multiplication by $I_0 d\theta = I_0 \omega dt$, and using equation (14) the specific torques are converted to differential energies:

$$-Mgl_{\text{com}} \sin\theta d\theta - \mathcal{T}_{\text{diss}} d\theta = \left(1 + \frac{3}{2}(\tau\omega)^2\right) I_0 \omega d\omega. \quad (22)$$

Upon integration and using the conveniently chosen integration constant $E - Mgl_{\text{com}}$, we obtain an energy equation:

$$Mgl_{\text{com}}(1 - \cos\theta) + E_{\text{diss}} + \frac{1}{2}I_0 \left(1 + \frac{3}{4}(\tau\omega)^2\right)\omega^2 = E \quad (23)$$

where E is the total energy of the system and E_{diss} is the dissipated energy (this makes the mechanical energy $E_{\text{mech}} = E - E_{\text{diss}}$). Given that the gravitic potential energy may be defined relatively to the lowest equilibrium point as

$$E_p = Mgl_{\text{com}}(1 - \cos\theta) \quad (24)$$

and presenting the maximum

$$E_{\text{pMAX}} = 2Mgl_{\text{com}} = 2I_0\Omega_0^2, \quad (25)$$

then the remaining term is the kinetic energy

$$E_k = \frac{1}{2}I_0 \left(1 + \frac{3}{4}(\tau\omega)^2\right)\omega^2 = \frac{1}{2}I_0\omega^2 + \frac{3}{8}I_0\tau^2\omega^4. \quad (26)$$

This means that the kinetic energy of the physical pendulum has one term associated with the moving rigid body

$$E_{\text{rig}} = \frac{1}{2}I_0\omega^2 \quad (27)$$

and another term associated with the moving surrounding air

$$E_{\text{air}} = \frac{3}{8}I_0\tau^2\omega^4. \quad (28)$$

This is similar to situations involving a component of pseudowork-energy balance in dissipative systems [73–79].

Using equation (25), equation (23) may be written in the following normalized form $\mathcal{E} = \frac{E}{E_{\text{pMAX}}}$

$$\mathcal{E} = \left(\sin\frac{\theta}{2}\right)^2 + \left(\frac{\omega}{2\Omega_0}\right)^2 + \left(\sqrt{3}\tau\omega\frac{\omega}{2\Omega_0}\right)^2 + \frac{E_{\text{diss}}}{E_{\text{pMAX}}}. \quad (29)$$

From the above equation the normalized mechanical energy (written like a three-dimensional Pythagorean Theorem) is:

$$\mathcal{A}^2 = \mathcal{A}_\theta^2 + \mathcal{A}_\omega^2 + \mathcal{A}_{\text{air}}^2. \quad (30)$$

where $\mathcal{A} = \sqrt{\mathcal{E}_{\text{mech}}} = \sqrt{\mathcal{E} - E_{\text{diss}}/E_{\text{pMAX}}}$, $\mathcal{A}_\theta = \sin(\theta/2)$, $\mathcal{A}_\omega = \omega/(2\Omega_0)$ and $\mathcal{A}_{\text{air}} = \sqrt{3\tau\omega\mathcal{A}_\omega}$. In view of the fact that $\mathcal{A}_{\text{air}}^2$ is likely to be very small, and also that equation (6) is just an approximation, we choose to consider

$$\mathcal{A}^2 \approx \mathcal{A}_\theta^2 + \mathcal{A}_\omega^2. \quad (31)$$

It is interesting to note that the above equation allows for a critical angular velocity

$$\omega_c = 2\Omega_0 \quad (32)$$

for which the maximum kinetic energy exceeds the maximum potential energy thus separating the oscillatory regime from the rotational motion [26, 80]. Also, equation (31) provides a way to define the instantaneous phase ϕ of the pendular motion as

$$\tan \phi = \frac{\mathcal{A}_\theta}{\mathcal{A}_\omega}. \quad (33)$$

As a consequence, the phase speed $\frac{d\phi}{dt}$ is

$$\Phi = \frac{\frac{d\mathcal{A}_\theta}{dt}\mathcal{A}_\omega - \mathcal{A}_\theta\frac{d\mathcal{A}_\omega}{dt}}{\mathcal{A}_\theta^2 + \mathcal{A}_\omega^2} = \frac{(\cos \frac{\theta}{2})\frac{\omega^2}{4\Omega_0} - (\sin \frac{\theta}{2})\frac{\alpha}{2\Omega_0}}{(\sin \frac{\theta}{2})^2 + \left(\frac{\omega}{2\Omega_0}\right)^2}. \quad (34)$$

B. Dissipation, inertia and negative damping

In addition to the viscous or Stokes drag, usually used in damped harmonic motion, Coulomb dry-friction and turbulent or Newton drag are also included in the standard dissipative acceleration expression [42, 48, 81–86]:

$$\alpha_{\text{diss}_s} = -C_1\omega - \frac{C_0 + C_2\omega^2}{\text{sgn}(\omega)} \quad (35)$$

where

$$\text{sgn}(x) = \begin{cases} 1 & \Leftarrow x \geq 0 \\ -1 & \Leftarrow x < 0 \end{cases} \quad (36)$$

Negative damping can be perceived as positive forcing [87–90] that happens whenever $\alpha + \Omega_0^2 \sin \theta$ has the same sign of ω , that is, the conditions observed in the odd quadrants of Figure 4 (highlighted in Figure 17).

For strictly dissipative torques, $\alpha + \Omega_0^2 \sin \theta = \alpha_{\text{diss}}$, negative damping can't be observed. However, in view of the inertial torque, the condition for negative damping is

$$(\alpha_{\text{diss}} + \alpha_{\text{iner}})\omega > 0. \quad (37)$$

Given the α_{diss} and α_{iner} expressions, it is clear both that, for positive angular velocity, the sum $\alpha_{\text{diss}} + \alpha_{\text{iner}}$ can only be positive for positive quadratic coefficient, i.e. $C_a \sin \theta - C_2 > 0$, and that, for angular velocities close to zero, negative damping is never observed due to the non-null Coulomb friction.

It is important to note that this result is counter-intuitive since the moving air, surrounding the pendulum, should contribute with positive forcing at near-zero speeds. From this point of view, the classical description of the dissipative and inertial torques doubtly will account for the detailed description of the pendular motion in particular for angular velocities close to zero. In fact, in Figure 4, one can observe typical characteristics of hysteresis and, close to null speed, positive forcing.

IV. CLASSIC MODEL

The standard dissipative acceleration α_{diss_s} , equation (35), is a parabolic function of angular velocity ω [91]. Some authors have used power-laws [30, 61, 92–97]. In order to test if such models provide better fits we considered the following power-law

$$\alpha_{\text{diss}_p} = -\frac{C_0 + C_3 \left| \frac{\omega}{\Omega_0} \right|^p}{\text{sgn}(\omega)}. \quad (38)$$

We verified that, although $\alpha_{\text{diss}_p}(\omega)$ contains a null slope of at zero speed, it does in fact allow better fits. Note that this feature bypasses all considerations concerning the mathematical expression of low speed friction [98, 99].

So, the classic model used is

$$\begin{aligned} \alpha + \Omega_0^2 \sin \theta &= \alpha_{\text{iner}} + \alpha_{\text{diss}_p} \\ &= C_a \omega^2 \sin \theta - \frac{C_0 + C_3 \left| \frac{\omega}{\Omega_0} \right|^p}{\text{sgn}(\omega)}. \end{aligned} \quad (39)$$

A. Classic model results

We used Fitteia [100] to fit the classic model §IV and the OPA model §V. Fitteia is a powerful fitting and plotting online platform that fulfills most of the requirements suggested in [101].

The classic model, equation (39), matches quite accurately all our experimental data. An example is given in Figure 8 (also see Figures 19 and 20).

We expected the classic model to provide clear results for C_a , the inertial or added-mass parameter that we introduced, but that's not so much the case. The complete set of obtained C_a values is presented in Figure 7. We expected C_a to increase when l_1 increases but this is only apparent for alley runs (1a and na). Also only the three highest tiles show different C_a between alley and no alley runs.

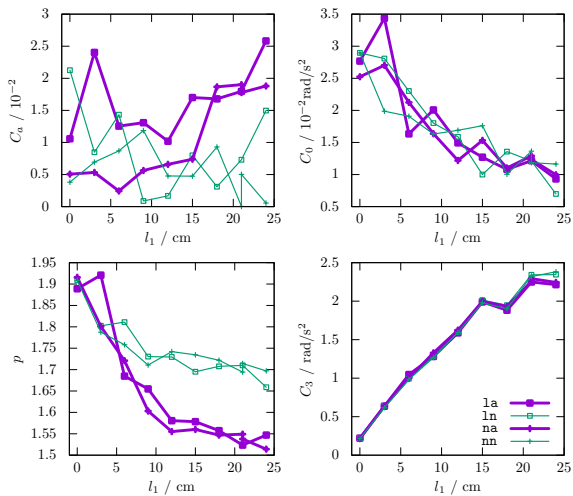


FIG. 7. Results from the classic model for parameters C_a , C_0 , p and C_3 . The obtained values of C_a prove that, in fact, equation (15) is valid because $(\tau\omega)^2 = \frac{2C_a\omega^2}{3\Omega_0^2} = \frac{8C_a}{3}\mathcal{A}_\omega^2 < \frac{8C_a}{3} < 0.08$. The results from the classic model for Ω_0 were very much confirmed by the fractional model and can therefore be observed in Figure 16.

The results for C_0 are more consistent (also shown in Figure 7). We think that the decrease of C_0 on increasing l_1 is caused by the larger tiles making very small and very slow oscillations disappear.

The most interesting results are those of p (also shown in Figure 7). It is clear that there is a difference between runs with alley and runs without alley. This difference can only be detected for the larger tiles and shows that the alley reduces turbulence.

The results for C_3 are very clear (also shown in Figure 7) showing almost linear increase with l_1 and independence of the alley. Note that if we had chosen the standard dissipative acceleration α_{diss} , equation (35), it would be C_2 to measure the importance of turbulence [84] and not p in equation (38).

We conclude that the classic model is generally very satisfactory as it can generally identify which runs used the alley and which runs did not. However, the classic model sometimes deviates a little from the first few swings of the pendulum and, furthermore, the classic model seems unable to eliminate a persistent dephasing or spurious oscillation visible in the residuals of the fits as, for instance, in Figure 8. Spurious oscillations are a long-standing problem in engineering and are usually associated with delayed action and self-oscillations [90, 102].

V. OPA MODEL

Pulse stretching and compression are two of the most crucial stages in chirped pulse amplifiers. Although chirped pulse conventional amplification (CPA) systems

have enabled the development of high-energy few-cycles pulses, an alternative technique for the generation of high-energy ultrashort pulses results from a combination of the CPA' stages with optical parametric amplification (OPA), which is a nonlinear optical phenomena [103–105], has been used. The conjugation of CPA with a nonlinear three-wave-mixing process, occurring within an adequate non-linear crystal where a stronger and higher frequency input wave (pump pulse) *exchanges energy* with a weaker and lower frequency input wave (seed pulse), generates an output signal pulse and also an auxiliary wave (idler pulse) due to energy and moment conservation (see Figure 9).

In this context we have found an interesting analogy between the physical pendulum relaxation (§III A) and the amplification of chirped laser pulses [106, 107]. Specially interesting is the similarity between our Figure 10 and the numerical solutions of the equations relating the pump A_p and the seed A_s amplitudes:

$$\frac{dA_p}{d\zeta} = \frac{\zeta B A_s}{4} \quad (40)$$

$$\frac{dA_s}{d\zeta} = -\frac{2A_s + 2B^* A_p}{\zeta} \quad (41)$$

$$\frac{dB}{d\zeta} = -\frac{\zeta A_p A_s^*}{2} \quad (42)$$

where B is density of states and ζ is a self-similar coordinate. Within this analogy the amplitudes of the pump pulse and the seed pulse correspond respectively to the amplitudes \mathcal{A}_θ and \mathcal{A}_ω of the energies involved in the movement of the pendulum, suggesting an explanation/understanding of the motion of the pendulum as it happens with OPA. This analogy can be made mathematically explicit:

$$A_p \equiv \mathcal{A}_\theta \quad (43)$$

$$A_s \equiv j\mathcal{A}_\omega \quad (44)$$

$$B \equiv -j\Phi' \quad (45)$$

$$\zeta \equiv \sqrt{t} \quad (46)$$

where $j = \sqrt{-1}$ and Φ' is a phase speed similar but not equal to the phase speed defined in equation (34). Equations (40), (41) and (42) are, therefore, analogous to

$$\frac{d\mathcal{A}_\theta}{dt} = \Phi' \mathcal{A}_\omega \quad (47)$$

$$\frac{d\mathcal{A}_\omega}{dt} = -\frac{C_4 \mathcal{A}_\omega + \Phi' \mathcal{A}_\theta}{t} \quad (48)$$

$$\frac{d\Phi'}{dt} = -\Omega_0^2 \mathcal{A}_\theta \mathcal{A}_\omega \quad (49)$$

where we have included the coefficient C_4 for generality. It's quite curious that equations (47), (48) and (49) can be understood as equations of either energy transfer or amplitude exchange where phase speed Φ' plays the role of exchange rate (analogous to density of states B). The

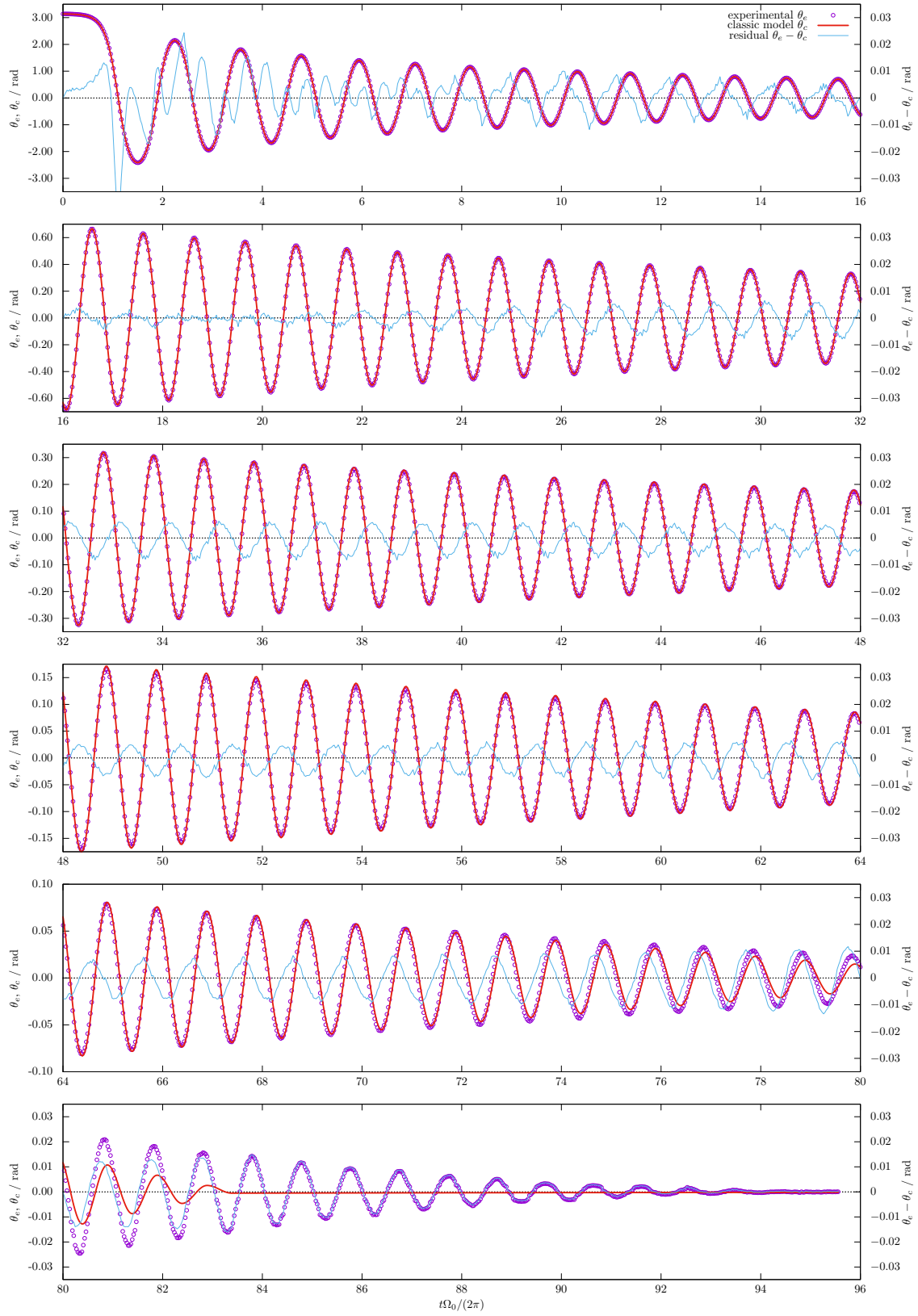


FIG. 8. Results for θ corresponding to run 03na1 fitted by the classic model. The complete run is shown to reveal the persistent spurious dephasing between the data and the model.

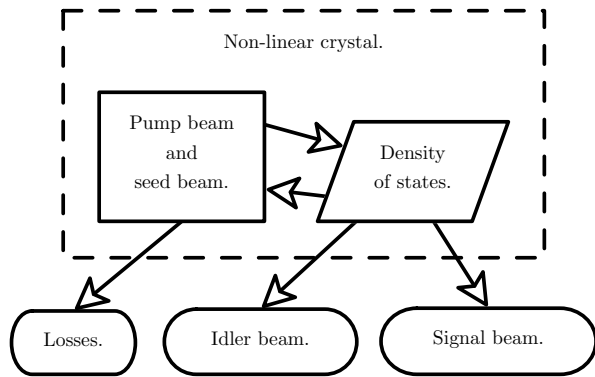


FIG. 9. Schematics of the energy exchanges taking place during optical parametric amplification. The process of parametric light amplification is a process occurring in the presence of a non-linear crystal. Most of the input energy, which is given by the pump beam, is used/converted to an increase of density of states and therefore increasing the intensity of the signal beam. Some pump energy is recovered and lost and the remaining part is used in the idler beam. Compare with Figure 6.

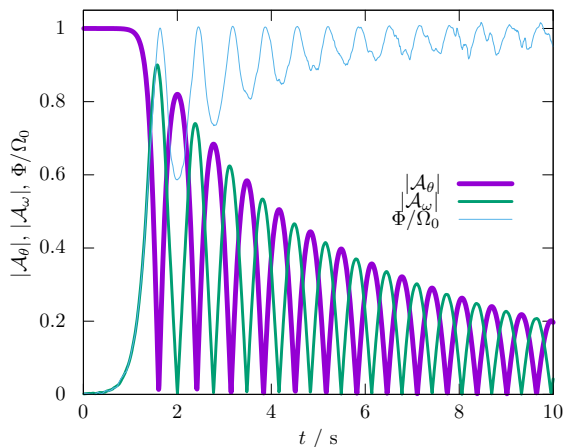


FIG. 10. Results for \mathcal{A}_θ and for \mathcal{A}_ω corresponding to run 24na1 fitted by the classic model. The obtained parameter values of Ω_0 and C_a were used to calculate \mathcal{A}_ω and the phase speed Φ (from equation 34). Note the noise propagated into the calculation of Φ .

explicit appearance of time t in one of the equations and their bad fit of the data led us to try a variety of similar sets of equations. We finally arrived at the following compromise between smallest modification and best fit:

$$\frac{d\mathcal{A}_\theta}{dt} = \Phi' \mathcal{A}_\omega \quad (50)$$

$$\frac{d\mathcal{A}_\omega}{dt} = -\frac{C_4 \mathcal{A}_\omega}{t} - \Phi' \mathcal{A}_\theta - \text{sgn}(\mathcal{A}_\omega) C_5 \quad (51)$$

$$\frac{d\Phi'}{dt} = -\Omega_0^2 \mathcal{A}_\theta \mathcal{A}_\omega \quad (52)$$

where we see that there is an additional coefficient (C_5) to account for Coulomb friction. Given that $\omega = \frac{d\theta}{dt}$ is

equivalent to

$$\frac{d\mathcal{A}_\theta}{dt} = \cos \frac{\theta}{2} \mathcal{A}_\omega \Omega_0, \quad (53)$$

equation (50) implies that

$$\Phi' = \Omega_0 \cos \frac{\theta}{2}. \quad (54)$$

This makes equation (51) exactly equivalent to

$$\frac{d\omega}{dt} + \frac{2\Omega_0 C_5}{\text{sgn}(\omega)} + \frac{C_4}{t} \omega + \Omega_0^2 \sin \theta = 0 \quad (55)$$

which is the equation of motion of a pendulum damped by both Coulomb friction and a laminar drag that changes with time. This $C_4 \omega/t$ term provides the required hysteretic behaviour but, once again, there is no provision for negative damping.

The analogy between the non-linearities of the pendulum and non-linear optics was also noted in reference [108]. Regarding analogies between a forced harmonic oscillator and non-linear optics see [109, 110].

A. OPA model results

Equations (50), (51), and (52) allow for quite good fits. Figure 11 presents one example. Many of OPA model fits show a 5% residual peak near $t = 1$ s similarly to the classic model (as in Figure 8).

The explicit inverse dependence on time (t^{-1}) in equation (51) obviously imposes an hyperbolic amplitude decay matching the experimental data for initial times.

As the OPA model can't describe negative damping, we resume its study and keep the idea that the experimental data is consistent with energy storage and converted energy release (parametric amplification that is similar to either self-oscillations or parametric pumping). So, now we have two models that fit our data but not in a completely satisfactory way. We continue investigating better models.

VI. FRACTIONAL DERIVATIVES

One common example, often used to introduce the concept of memory, is what happens when the air and dust entrained by a moving car, on a desert sandy road, ends up overcoming and falling on the wind-shield when the car slows down to a full stop. This intuitive event, representing a memory effect of the whole system, can also be observed in underwater pendula [52].

Memory effects are an integration of past events (history) and, in the case of a physical pendulum, cannot be modelled exclusively by an added mass that depends on the instantaneous only θ and ω (see Figure 17). Memory

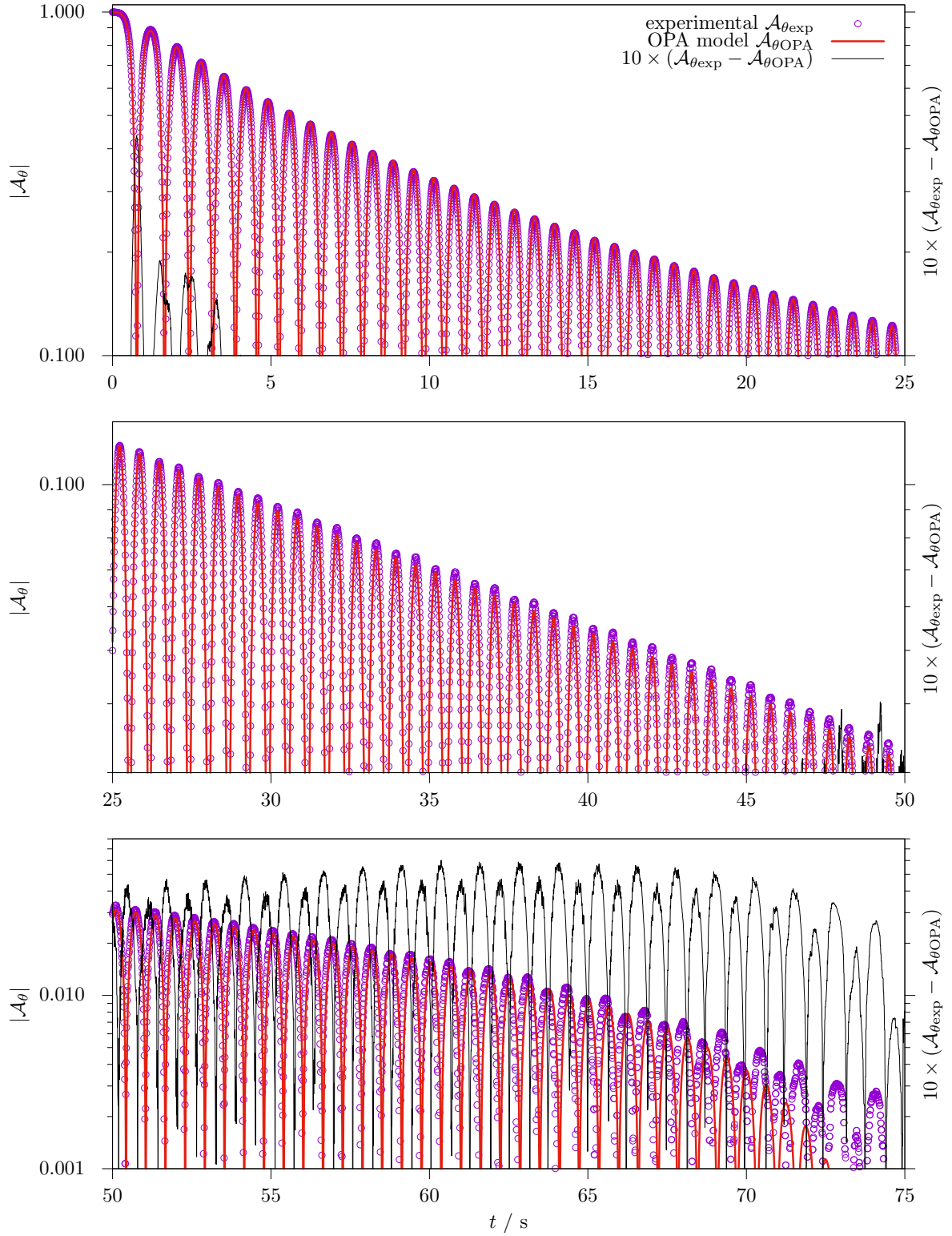


FIG. 11. Results for \mathcal{A}_θ corresponding to run 091a1 fitted by the OPA model. Fitted parameter values are $\Omega_0 = 5.05 \text{ rad s}^{-1}$, $C_4 = 3.25$, $C_5 = 1.57 \times 10^{-3} \text{ s}^{-1}$, and $t_0 = -8.85 \text{ s}$ (this is the zero of model time in the experimental time scale).

effects are traditionally described by the Basset history force [111–122]

$$F_H = \frac{3}{2} \rho d_s^2 \sqrt{\pi \nu} \int_0^t a(t') \frac{dt'}{\sqrt{t-t'}} \quad (56)$$

where ρ is the fluid specific mass, d_s is the diameter of a sphere, ν is the kinematic viscosity and a is the translational acceleration of the sphere in the stationary fluid. The expression of the Basset force is equivalent to a fractional semi-derivative [123–126]

$$F_H \propto \mathcal{D}_t^{\frac{1}{2}} v, \quad (57)$$

where v is the translational velocity of the sphere in the stationary fluid. The above semi-derivative can be generalized

$$F_H \propto \mathcal{D}_t^\beta v \quad (58)$$

establishing a connection between the fractional derivative order and the permanence of memory [127]. The above constitutes a sound basis for the introduction of a fractional derivative in the physical pendulum equation of motion. Nevertheless, there is a diversity of reasons, listed below, that provide additional support.

1. Fractional derivatives integrate all causes of memory effects and may, therefore, be used either as a replacement of those causes [128] or as a completion of a rough model [129].
2. Fractional models can describe negative damping [130], mechanical energy increases, and/or odd-even symmetry breakings [131, 132].
3. Significant reductions in the number of model parameters was achieved in viscoelasticity [133–136], thermal systems [137], acoustics [138], electronics [139], and biology [140].
4. The equivalence between differential equations of non-integer order with a constant coefficient and differential equations of integer order with a varying coefficient, like equation (55), has been conjectured [141, 142].
5. Additional memory terms were found necessary for the BBO equation [143–146] both when extended to compressible fluids [121, 147] and when considering axisymmetric bodies [148].
6. The Basset history force was found non-negligible in oscillatory motion [149].
7. The term $-(\tau\omega)^2\alpha$ in equation (10) was identified as a “*summary of the history integral effect*” [57].

Taking all these reasons into consideration, we introduce in section §VII a fractional differential equation of motion for the physical pendulum.

We shall use a time-independent-order fractional derivative but note that some authors prefer variable-order [150, 151].

A few aspects of fractional derivatives, related to their widespread use, are mentioned next.

The fractional derivative provides a functional interpolation between closest integer derivatives. Figure 12 contains examples.

The fractional derivative of a trigonometric function is proportional to a dephasing of the original function and the amount of dephasing is itself proportional to the order of the fractional derivative.

Fractional derivatives have been studied for a long time and were defined in many ways but became an instrument of physicists only recently and therefore their physical meaning has been the subject of several discussions [152–154], particularly in respect of projectile motion [155, 156] and damped harmonic motion [157].

Recently, an early introduction of fractional calculus syllabus was proposed [158].

A. Calculating fractional derivatives

Our calculations are based on the Grünwald-Letnikov definition of fractional derivative [159] which is considered a fractional derivative in a strict sense [160]. As time fractional derivatives must be calculated from past data only (ignoring future data) for causality to be kept, a time fractional derivative must be a left derivative. Consider a function $f(t)$, where t is time, which is known only at a discrete set of steps $t_i = t_{i-1} + h$, $i = 0, \dots, N$ so that $f_i = f(t = t_i)$. Consider also that the time fractional derivative of order β corresponds to the operator \mathcal{D}_t^β . Then we use

$$\left(\mathcal{D}_t^\beta f\right)_i = \frac{1}{h^\beta} \sum_{k=0}^N W_k f_{i-k} \quad (59)$$

where

$$W_k = \left(1 - \frac{\beta + 1}{k}\right) W_{k-1}, \quad W_0 = 1,$$

$h = 1/120$ s, coinciding with the videos’ frame rate, and $N = 100$ (we take one hundred steps into the past to calculate the fractional derivative). This means that $Nh \approx T$ where T is the oscillation period.

B. Solving fractional differential equations

As for solving integer differential equations, fractional differential equations require adequate numerical methods. Following some preliminary tests with the compact numerical method proposed by Seredyńska and Hanyga [161] to solve fractional differential equations for nonlinear oscillators, a version of the algorithm proposed by

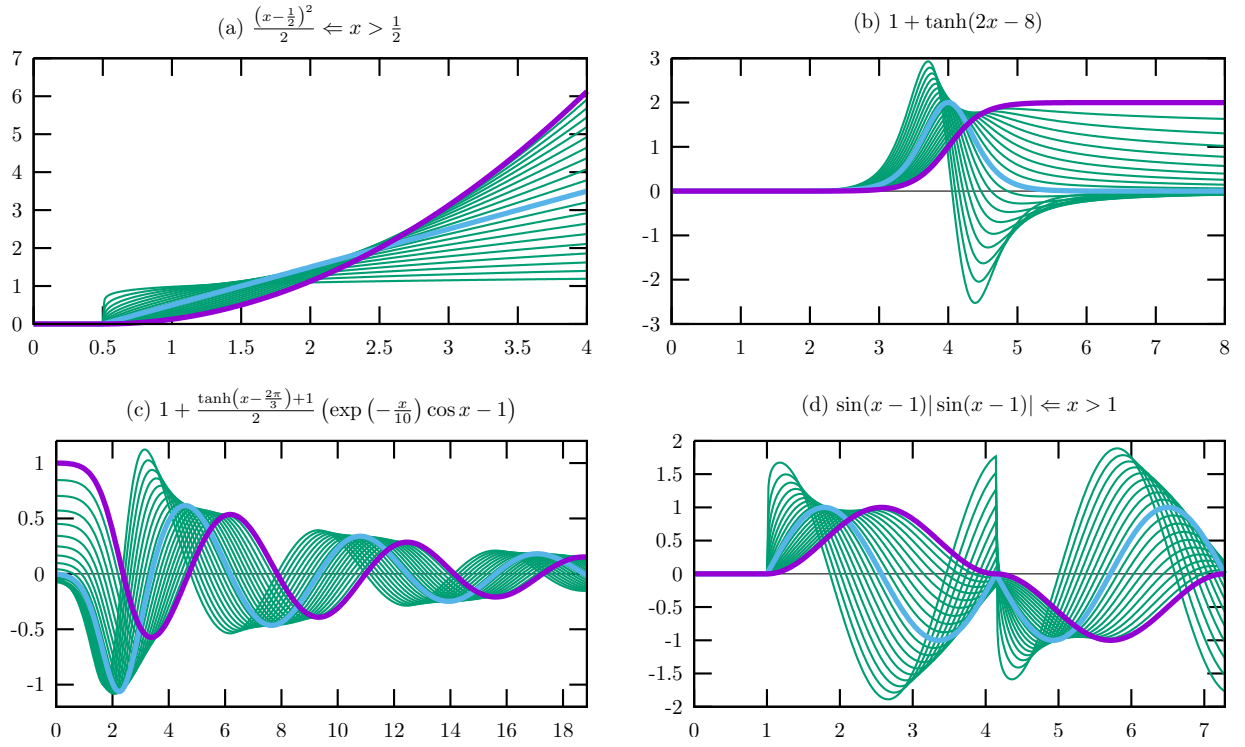


FIG. 12. Plots of four functions in purple, first derivatives in blue and left Grünwald-Letnikov fractional derivatives of order $\beta = 0.1, 0.2, \dots, 1.9$ in green as calculated by equation (59) with $h = (x \text{ range})/700$ and $N = 500$ for (a) and (b) or $N = 100$ for (c) and (d).

Spanos and Evangelatos [162] was implemented because it generally follows the principles of predictor-corrector methods [163].

A general pendulum equation of motion may be written as (§VII)

$$\alpha + \Omega_0^2 \sin \theta = \alpha_{dl} + \mathcal{D}_t^\beta \alpha_{dh} \quad (60)$$

where α_{dl} is a known algebraic function of the angular velocity describing dissipative acceleration at low speed and α_{dh} is a known algebraic function of the angular velocity describing dissipative acceleration at high speed but ignoring memory effects. Supposing known initial angle θ_0 , angular velocity ω_0 and angular acceleration α_0 , the method starts by making a prediction about some values of the next step using a Taylor series expansion

$$\theta_{i+1} = \theta_i + \left(\omega_i + \alpha_i \frac{h}{2} \right) h \quad (61)$$

$$(\sin \theta)_{i+1} = \sin \theta_i + \left(\omega_i \cos \theta_i + (\alpha_i \cos \theta_i - \omega_i^2 \sin \theta_i) \frac{h}{2} \right) h \quad (62)$$

$$\omega_{i+1} = \omega_i + \alpha_i h \quad (63)$$

$$\alpha_{dh_{i+1}} = \alpha_{dh_i} + \left. \frac{d\alpha_{dh}}{d\omega} \right|_i \alpha_i h \quad (64)$$

The history sum is

$$\Sigma_{i+1} = \sum_{k=1}^N W_k \alpha_{dh_{i+1-k}}$$

and the fractional derivative is, therefore, predicted to be

$$\left(\mathcal{D}_t^\beta \alpha_{dh} \right)_{i+1} = \frac{\alpha_{dh_{i+1}} + \Sigma_{i+1}}{h^\beta}.$$

The angular acceleration results from equation (60)

$$\alpha_{i+1} = -\Omega_0^2 (\sin \theta)_{i+1} + \alpha_{dl_{i+1}} + \left(\mathcal{D}_t^\beta \alpha_{dh} \right)_{i+1}. \quad (65)$$

The method continues by correcting the predictions via the linear acceleration approximation [164]

$$\theta_{i+1} = \theta_i + \left(\omega_i + (2\alpha_i + \alpha_{i+1}) \frac{h}{6} \right) h \quad (66)$$

$$\omega_{i+1} = \omega_i + (\alpha_{i+1} + \alpha_i) \frac{h}{2} \quad (67)$$

and finishes reapplying equation (65).

In order to avoid numerical ambiguities related with initial conditions we assumed that the pendulum was placed or launched at constant velocity, that is, we assumed null acceleration on the whole unknown past [165, 166]. Note that the Grünwald-Letnikov definition is, in this case, equivalent to the original Riemann-Liouville definition [167].

VII. FRACTIONAL MODEL

Given the unclear results of $C_a(l_1)$ in Figure 7 and the absence of negative damping in results of both the classic model and the OPA model, we opted for replacing α_{iner} , equation (18), with a fractional derivative. The introduction of a fractional derivative made us try to non-dimensionalize the equation of motion in order avoid changing units. This is achieved dividing by $(2\Omega_0)^2$. A long trial-and-error process finally led us to the following fractional model.

$$\frac{d\mathcal{A}_\omega}{dt^*} + \frac{\sin \theta}{4} = -\frac{G_1 \sqrt[4]{|\mathcal{A}_\omega|}}{\text{sgn}(\mathcal{A}_\omega)} - G_2 \mathcal{D}_{t^*}^\beta (\mathcal{A}_\omega |\mathcal{A}_\omega|^{p_f-1}) \quad (68)$$

where $t^* = 2\Omega_0 t$ is a non-dimensional time and $\mathcal{D}_{t^*}^\beta$ is the left Grünwald-Letnikov fractional derivative of order β in t^* . Note that

$$\mathcal{A}_\omega = \frac{d\theta}{dt^*} = \mathcal{D}_{t^*}^1 \theta. \quad (69)$$

Also note that $G_1 \sqrt[4]{|\mathcal{A}_\omega|}$ is similar to the friction proposed in [168].

A. Fitting models to data

We used `amebsa` [169], almost completely reimplemented in PASCAL language to fit the fractional model §VII (with initial estimates guided by the classic model).

Fitting is in this case an iterative process and, therefore, depends on an initial estimate of the model parameters. In order to calculate parameter uncertainties one must generate a sample of best-fitting parameter sets. We generated 150 best-fitting parameter sets of the fractional model (§VII) for each experimental data run. Each individual parameter set was obtained from a single fitting procedure, each with a different initial estimate selected randomly from a range set. A single range set was defined by previous fitting trial-and-error for each experimental data run. This trial-and-error means is-or-is-not in the basin of attraction to the global best-fitting parameter set. Out of each sample of 150 individual parameter sets, we identified the one corresponding to the minimum of

$$\Xi^2 = \frac{1}{N} \sum_{i=1}^N \left((\mathcal{A}_{\theta \text{mod}} - \mathcal{A}_{\theta \text{exp}})^2 + (\mathcal{A}_{\omega \text{mod}} - \mathcal{A}_{\omega \text{exp}})^2 \right) \quad (70)$$

where N is the number of experimental data points of the run. This minimum is Ξ_{min}^2 . We then selected the parameter sets having $\Xi^2 \leq \frac{5}{4} \Xi_{\text{min}}^2$. From this selection we identified the maximum Ψ_{max} and the minimum Ψ_{min} of each parameter Ψ . Finally, we calculated the uncertainty as

$$u(\Psi) = \frac{\Psi_{\text{max}} - \Psi_{\text{min}}}{2}. \quad (71)$$

The uncertainties thus calculated appear in figures 15 and 16.

B. Fractional model results

Our main result is the long-time accurate fit of experimental data for all runs. In Figure 13 we present the results obtained for the best fit of run `03na1`, as an example, showing that apparent mismatch between fit and data occurs only in the last fifth of oscillation time. An alternative 3D representation, corresponding to equations (70), (31) and (33) is presented in Figure 14. This figure highlights a curious feature of launched runs: phase velocity changes sign when $\theta = \pi$ rad.

The results for the fractional derivative order β in Figure 15 allow an easier interpretation than those for C_a in Figure 7. The high uncertainties of β do not hide the fact that there are two behaviours: one for small tiles and another for big tiles. Small tiles imply near zero memory effects for launched runs and big tiles imply that the alley increases the memory effects. Taken together these two behaviours say that memory effects are enhanced by low speed. As expected, the results for G_1 , G_2 and p_f in Figure 15 are qualitatively similar to the results for C_0 , C_3 and p in Figure 7. Note, however, that the derivative of a polynomial reduces its degree and, therefore, it would be expected that

$$p_f - \beta \approx p. \quad (72)$$

Finally, the results for Ω_0 in Figure 16 demonstrate the high accuracy of the fractional model both by the small relative uncertainties ($u_r < 0.3\%$) and by the good consistency with the independent theoretical model explained below. Figure 16 shows that Ω_0 is slightly lower for the alley runs. This is consistent with an augmented system's inertia and reveals the effect of the coherent air flowing along the alley lateral and bottom surfaces, specially in the small angle oscillations.

Assume that the pendulum and the tiles are perfect cuboids. Suppose that we assemble the pendulum of mass M_0 with one tile of mass m . We may now write

$$\Omega_0^2 = \frac{(M_0 l_{\text{com}} + mR)g}{I_0 + \left(R^2 + \frac{l_1^2}{12}\right) m} \quad (73)$$

where $R = l_0 - \frac{l_1}{2}$ and $I_0 = M_0 \frac{l_0^2}{3}$ (see Figure 1). Considering that $M_0 = \lambda_0 l_0$, $m = \lambda_1 l_1$ and $l_{\text{com}} = l_0/2$, where λ is mass per unit length assumed equal for all tiles, one arrives at

$$\Omega_0 = \sqrt{\frac{g}{l_0}} \sqrt{\frac{\frac{1}{2}X + \frac{l_1}{l_0} - \frac{1}{2} \left(\frac{l_1}{l_0}\right)^2}{\frac{1}{3}X + \frac{l_1}{l_0} - \left(\frac{l_1}{l_0}\right)^2 + \frac{1}{3} \left(\frac{l_1}{l_0}\right)^3}} \quad (74)$$

where $X = \lambda_0/\lambda_1$. We fitted this equation to the results of $\Omega_0(l_1)$ in Figure 16 and obtained $X \approx 1.48$ and

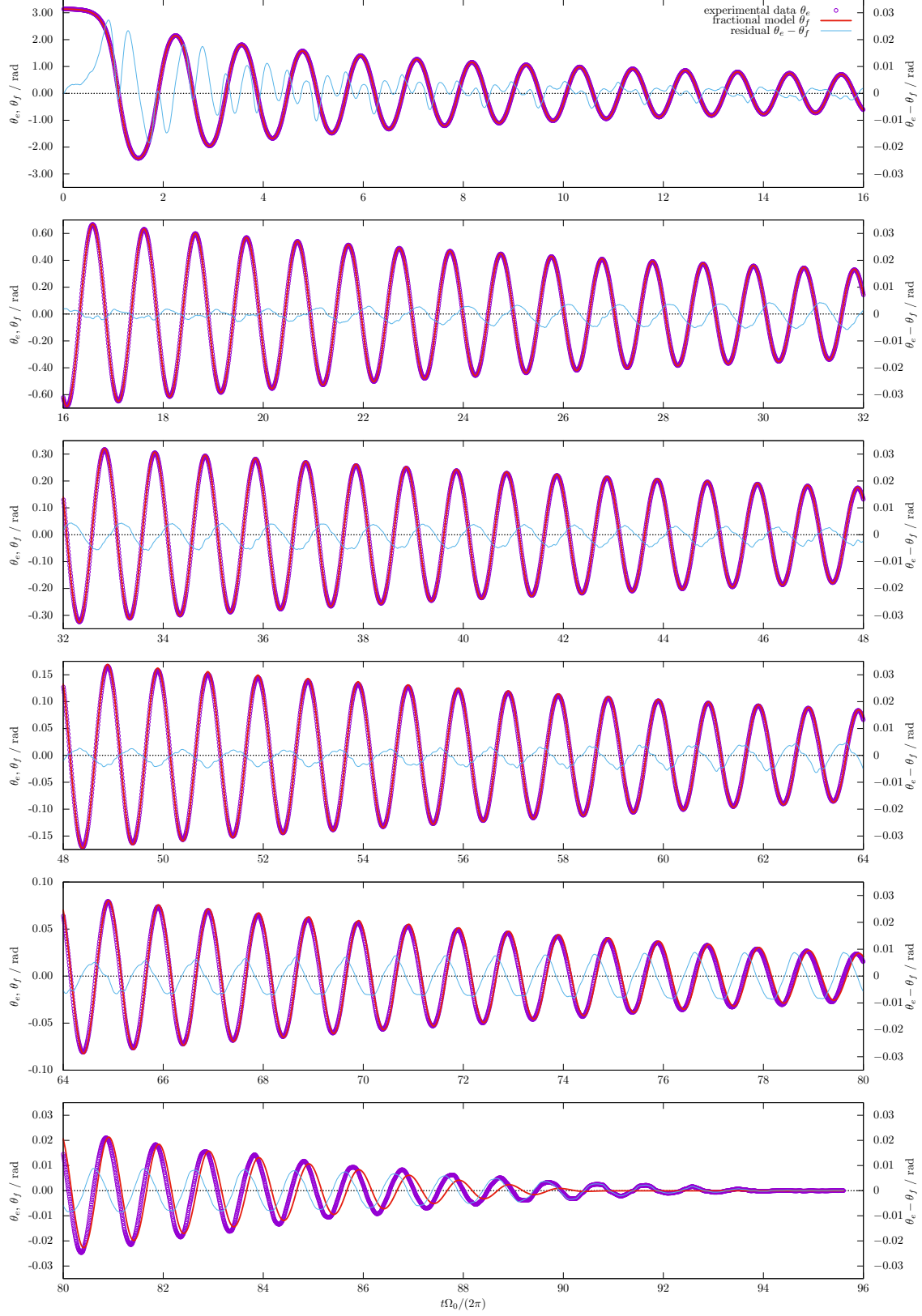


FIG. 13. Results for θ corresponding to run 03na1 fitted by the fractional model. Compare with Figure 8.

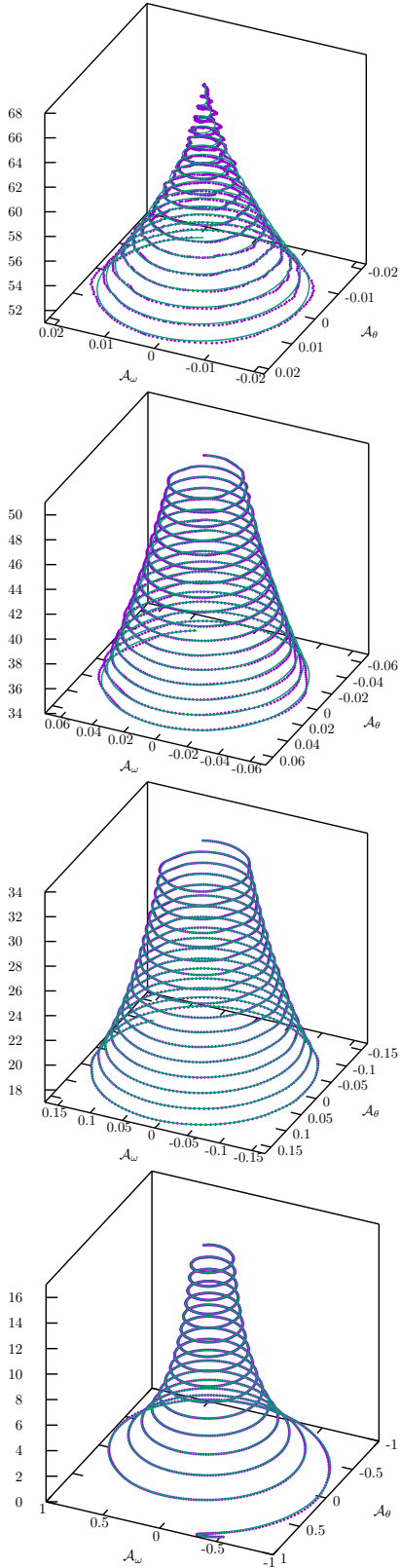


FIG. 14. Nyquist-like plots [170] with both experimental data points and fractional model corresponding to the fit of run 091n1. The vertical axis is time in units of natural period ($t\Omega_0/(2\pi)$).

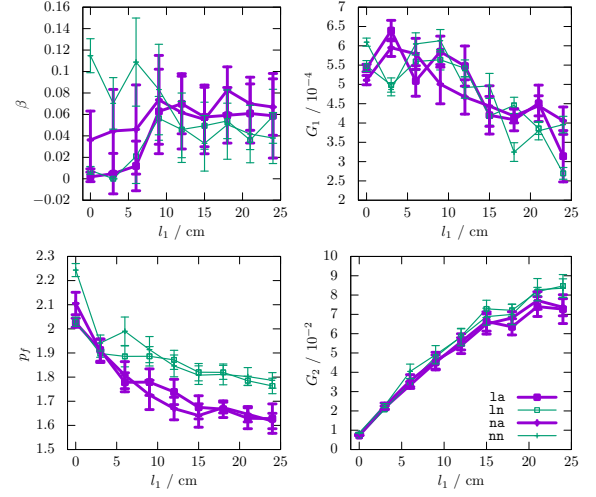


FIG. 15. Results from the fractional model for parameters β , G_1 , p_f and G_2 . Compare with Figure 7 noting that $G_1 \simeq \frac{C_0}{4\Omega_0^2}$ and $G_2 \simeq \frac{C_3}{2^{2-p}\Omega_0^2}$.

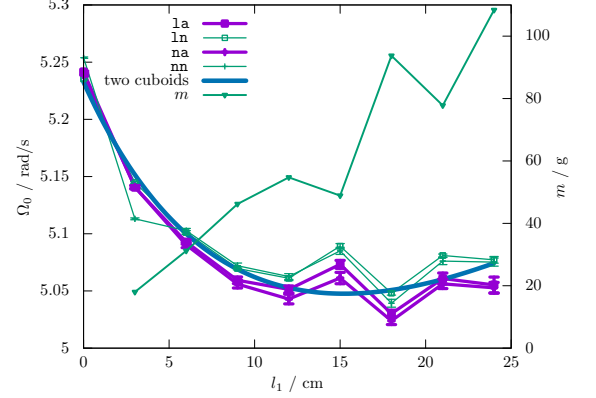


FIG. 16. Complete set of results from the fractional model for parameter Ω_0 . The “two cuboids” line is a fitting of equation (74). The mass m of each tile is also plotted.

$l_0 \approx 54$ cm. The actual value is 52 cm. The fitted and the actual l_0 values don’t match exactly because the actual pendulum isn’t a cuboid and the tiles don’t have equal mass per unit length. However, the results for Ω_0 in Figure 16 show that when $\lambda_1 = m/l_1$ increases, Ω_0 consistently decreases.

The set of results from the fractional model for run 241a1 allows the revisualization of Figure 4 as in Figure 17.

VIII. CONCLUSION

The physical pendulum is traditionally treated as a rigid body and a one-body equation is used to describe a rotating center of mass. Only gravitational and strictly dissipative torques are traditionally considered but the

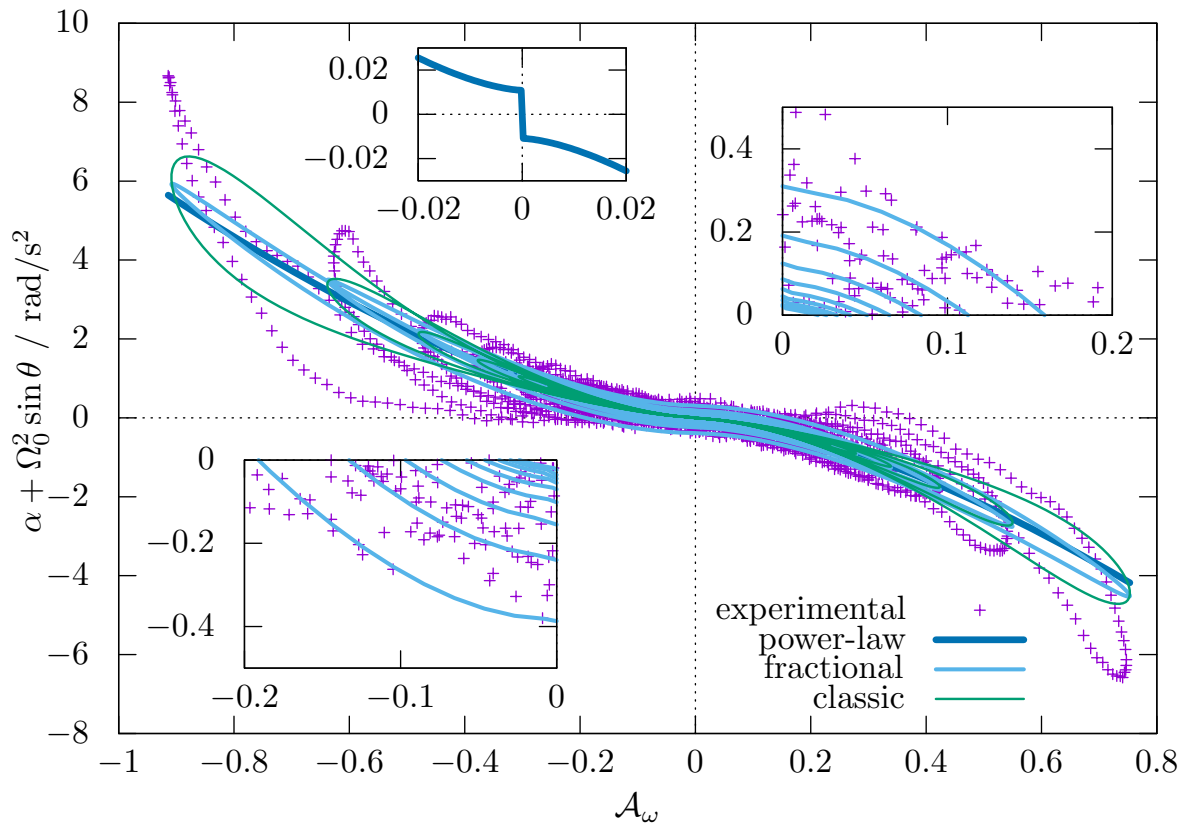


FIG. 17. Sum of the dissipative acceleration and the inertial acceleration for the initial ten seconds of the 241a1 run. Two insets show where dissipative acceleration and velocity have the same sign (negative damping). The fitted classic model does not describe negative damping (see top-left inset). Nevertheless, this plot shows that both the classic model and the fractional model reproduce a hysteretic dissipation. Equation (39) with $C_a = 0$ is indicated as “power-law”.

experimental data collected in this experiment clearly shows, for large amplitude oscillations, a hysteretic behaviour. Also, the experimental results confirm that a fixed structure unconnected to the pendulum may modify its motion. This means that the pendulum damping depends on the flow of air surrounding the pendulum. The pendulum equation of motion must, therefore, account for a multitude of air flow consequences, such as non-constant moment of inertia, recoverable air kinetic energy, automatic parametric pumping, and the compound hysteretic behaviour. The special consequence of non-null air flow when the strictly rigid pendulum stops, imposes the consideration of memory effects that can only be adequately modelled by fractional derivatives.

Some attention was paid to the extraction of another classic rigid body concept, the natural angular frequency of the linear harmonic oscillator. On the one hand, estimates of the natural angular frequency can be obtained directly from both angle and acceleration experimental data but, on the other hand, our model-based estimates

establish an interdependency between the use of an unconnected structure and the natural angular frequency.

Given the obtained results it is possible to expect not only that the proposed fractional model will be able to fit general pendular phenomena including forcing, amplitude resonance, and rotatory regime but also that the fractional derivative of a power-law can be used as a generic model of air drag.

The physical pendulum is, after all, the *exponent* of classics.

ACKNOWLEDGMENTS

We gratefully acknowledge enlightening discussions with Manuel Ortigueira, Arnaldo Baptista, Grégoire Bonfait, Carlos Dias, Carlos Cruz and Mendanha Dias. We also acknowledge the american english language revision by Jeffrey Keefer.

[1] H. Erlichson, *The Physics Teacher* **37**, 478 (1999).

[2] C. Huygens, *Horologium oscillatorium: sive de motu*

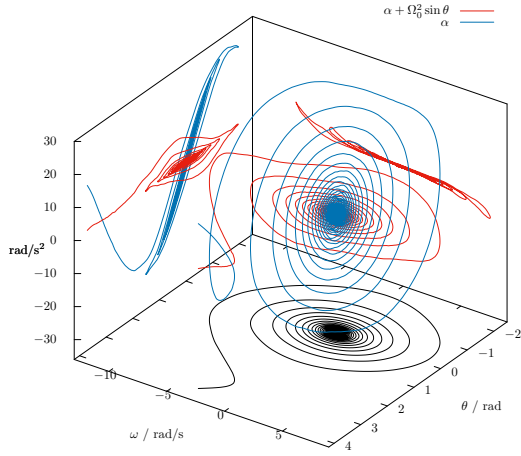


FIG. 18. Kinematic data for run 241a1.

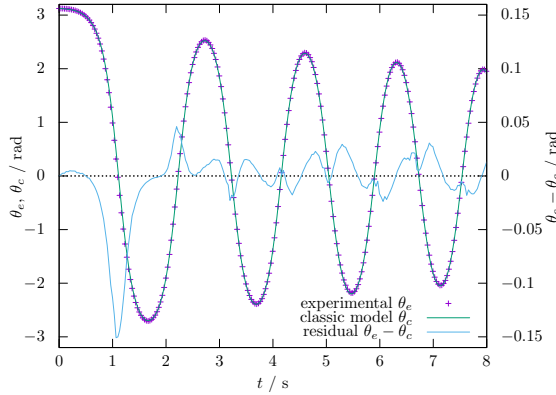


FIG. 19. Results for θ corresponding to run 00nn1 fitted by the classic model. Only the first few cycles are shown to reveal the single 5% residual peak near $t = 1$ s.

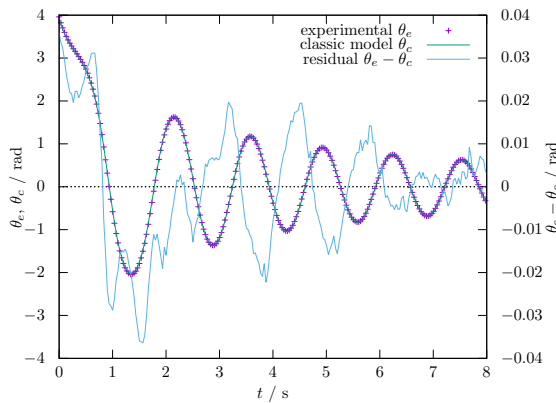


FIG. 20. Results for θ corresponding to run 181a1 fitted by the classic model. Only the first few cycles are shown to reveal the high accuracy of the fit.

pendulorum ad horologia aptato demonstrationes geometricæ (F. Muguet, 1966).

- [3] H. Kater and T. Young, *Philosophical Transactions of the Royal Society of London* **108**, 33 (1818).
- [4] J. E. Jackson, *Geophysical Journal International* **4**, 375 (1961), http://oup.prod.sis.lan/gji/article-pdf/4/Supplement_1/375/1833118/4-Supplement_1-375.pdf.
- [5] I. Marson and U. Riccardi, *International Journal of Geophysics* (2012), 10.1155/2012/687813.
- [6] D. G. Blair, L. Ju, and M. Notcutt, *Review of Scientific Instruments* **64**, 1899 (1993).
- [7] V. Mitrofanov and N. Styazhkina, *Physics Letters A* **256**, 351 (1999).
- [8] T. Uchiyama, T. Tomaru, D. Tatsumi, S. Miyoki, M. Ohashi, K. Kuroda, T. Suzuki, A. Yamamoto, and T. Shintomi, *Physics Letters A* **273**, 310 (2000).
- [9] G. Cagnoli, L. Gammaitoni, J. Hough, J. Kovalik, S. McIntosh, M. Punturo, and S. Rowan, *Phys. Rev. Lett.* **85**, 2442 (2000).
- [10] F. M. S. Lima, *European Journal of Physics* **29**, 1091 (2008).
- [11] J. R. Sanmartín, *American Journal of Physics* **52**, 937 (1984).
- [12] S. Wirkus, R. Rand, and A. Ruina, *The College Mathematics Journal* **29**, 266 (1998).
- [13] D. S. Stilling and W. Szyszkowski, *International Journal of Non-Linear Mechanics* **37**, 89 (2002).
- [14] A. A. Post, G. de Groot, A. Daffertshofer, and P. J. Beek, *Motor Control* **11**, 136 (2007).
- [15] J. A. Greenwood, K. L. Johnson, S.-H. Choi, and M. K. Chaudhury, *Journal of Physics D: Applied Physics* **42**, 035301 (2008).
- [16] M. Oblgado, M. Puy, and M. Bourgoïn, *Journal of Fluid Mechanics* **728**, R2 (2013).
- [17] R. Cuerno, A. F. Rañada, and J. J. Ruiz-Lorenzo, *American Journal of Physics* **60**, 73 (1992).
- [18] R. DeSerio, *American Journal of Physics* **71**, 250 (2003).
- [19] M. Ya. Azbel and P. Bak, *Phys. Rev. B* **30**, 3722 (1984).
- [20] F. J. Romeiras and E. Ott, *Phys. Rev. A* **35**, 4404 (1987).
- [21] G. J. Milburn and D. F. Walls, *American Journal of Physics* **51**, 1134 (1983).
- [22] B. Yurke, *American Journal of Physics* **54**, 1133 (1986).
- [23] D. Doubochinski and J. Tennenbaum, “The macroscopic quantum effect in nonlinear oscillating systems: a possible bridge between classical and quantum physics,” (2007), arXiv:0711.4892 [physics.gen-ph].
- [24] A. I. Shumaev and Z. A. Maizelis, *Journal of Applied Physics* **121**, 154902 (2017).
- [25] M. Pigneur and J. Schmiedmayer, *Phys. Rev. A* **98**, 063632 (2018).
- [26] J. Naudts, *Europhysics Letters (EPL)* **69**, 719 (2005).
- [27] M. Baeten and J. Naudts, *Entropy* **13**, 1186 (2011).
- [28] A. Lukichev, *Chemical Physics* **428**, 29 (2014).
- [29] A. Lukichev, *Journal of Non-Crystalline Solids* **420**, 43 (2015).
- [30] A. Lukichev, *Journal of Non-Crystalline Solids* **442**, 17 (2016).
- [31] A. Lukichev, *Physics Letters A* **383**, 2983 (2019).
- [32] A. B. Rabinovich, “Seiches and harbor oscillations,” in *Handbook of Coastal and Ocean Engineering*, pp. 193–236.
- [33] J. W. Fee, in *Proceedings of the IEEE 28th An-*

- nual Northeast Bioengineering Conference (IEEE Cat. No.02CH37342)* (2002) pp. 33–34.
- [34] R. D. Peters, “Nonlinear damping of the ‘linear’ pendulum,” (2003), arXiv:physics/0306081 [physics.class-ph].
- [35] J. C. Fernandes, P. J. Sebastião, L. N. Gonçalves, and A. Ferraz, *European Journal of Physics* **38**, 045004 (2017).
- [36] M. Kavyanpoor and S. Shokrollahi, *Journal of King Saud University - Science* **31**, 14 (2019).
- [37] M. Amabili, *Nonlinear Dynamics* **97**, 1785 (2019).
- [38] L. P. Fulcher and B. F. Davis, *American Journal of Physics* **44**, 51 (1976).
- [39] D. E. Hall and M. J. Shea, *American Journal of Physics* **45**, 355 (1977).
- [40] S. C. Zilio, *American Journal of Physics* **50**, 450 (1982).
- [41] S. Gil, A. E. Legarreta, and D. E. Di Gregorio, *American Journal of Physics* **76**, 843 (2008).
- [42] P. T. Squire, *American Journal of Physics* **54**, 984 (1986).
- [43] L. Basano and P. Ottonello, *American Journal of Physics* **59**, 1018 (1991).
- [44] L. F. C. Zonetti, A. S. S. Camargo, J. Sartori, D. F. de Sousa, and L. A. O. Nunes, *European Journal of Physics* **20**, 85 (1999).
- [45] X. jun Wang, C. Schmitt, and M. Payne, *European Journal of Physics* **23**, 155 (2002).
- [46] M. E. Bacon and D. D. Nguyen, *European Journal of Physics* **26**, 651 (2005).
- [47] J. C. Simbach and J. Priest, *American Journal of Physics* **73**, 1079 (2005).
- [48] B. R. Smith, *American Journal of Physics* **80**, 816 (2012).
- [49] C. E. Mungan and T. C. Lipscombe, *European Journal of Physics* **34**, 1243 (2013).
- [50] V. Mathai, L. A. W. M. Loeffen, T. T. K. Chan, and S. Wildeman, *Journal of Fluid Mechanics* **862**, 348–363 (2019).
- [51] Y. Eng, W. Lau, E. Low, and G. Seet, in *International MultiConference of Engineers and Computer Scientists*, Vol. 2 (2008) pp. 423–430.
- [52] D. Bolster, R. E. Hershberger, and R. J. Donnelly, *Phys. Rev. E* **81**, 046317 (2010).
- [53] S. Whineray, *European Journal of Physics* **12**, 90 (1991).
- [54] P. F. Hinrichsen and C. I. Larnder, *American Journal of Physics* **86**, 577 (2018).
- [55] E. Lorenceau, D. Quéré, J.-Y. Ollitrault, and C. Clanet, *Physics of Fluids* **14**, 1985 (2002).
- [56] R. P. Smith and E. H. Matlis, *American Journal of Physics* **87**, 433 (2019).
- [57] L. Basano and P. Ottonello, *American Journal of Physics* **57**, 999 (1989).
- [58] J. Alho, H. Silva, V. Teodoro, and G. Bonfait, *Physics Education* **54**, 015015 (2018).
- [59] C. I. Larnder, *American Journal of Physics* **87**, 784 (2019).
- [60] B. Mann and F. Khasawneh, *Journal of Sound and Vibration* **321**, 65 (2009).
- [61] N. Jakšić, *Journal of Sound and Vibration* **330**, 5878 (2011).
- [62] L. N. Gonçalves, in *Internatinoal Conference on TEX, XML, and Digital Typography* (Springer, 2004) pp. 112–124.
- [63] The color pink was chosen because it produced the best contrast.
- [64] D. Brown, “Tracker video analysis and modeling tool,” <http://physlets.org/tracker/>.
- [65] W. H. Press and S. A. Teukolsky, *Computers in Physics* **4**, 669 (1990).
- [66] E. Ermanyuk, *Experiments in fluids* **28**, 152 (2000).
- [67] D. Neill, D. Livelybrooks, and R. J. Donnelly, *American Journal of Physics* **75**, 226 (2007).
- [68] J. Messer and J. Pantaleone, *The Physics Teacher* **48**, 52 (2010).
- [69] J. Pantaleone and J. Messer, *American Journal of Physics* **79**, 1202 (2011).
- [70] N. Raza, I. Mehmood, H. Rafiuddin, and M. Rafique, in *Proceedings of 2012 9th International Bhurban Conference on Applied Sciences Technology (IBCAST)* (2012) pp. 270–273.
- [71] E. Konstantinidis, *Proceedings of the Royal Society A: Mathematical, Physical and Engineering Sciences* **469**, 20130135 (2013).
- [72] R. Peters, *Contemporary Physics* **45**, 475 (2004).
- [73] C. M. Penchina, *American Journal of Physics* **46**, 295 (1978).
- [74] J. Copeland, *American Journal of Physics* **50**, 599 (1982).
- [75] B. A. Sherwood, *American Journal of Physics* **51**, 597 (1983).
- [76] A. B. Arons, *American Journal of Physics* **67**, 1063 (1999).
- [77] J. Güémez and M. Fiolhais, *European Journal of Physics* **34**, 345 (2013).
- [78] J. Güémez and M. Fiolhais, *European Journal of Physics* **37**, 045101 (2016).
- [79] J. Güémez and M. Fiolhais, *European Journal of Physics* **39**, 045010 (2018).
- [80] F. M. S. Lima, *American Journal of Physics* **78**, 1146 (2010).
- [81] R. A. Nelson and M. G. Olsson, *American Journal of Physics* **54**, 112 (1986).
- [82] K. Takahashi and D. Thompson, *American Journal of Physics* **67**, 709 (1999).
- [83] A. Arora, R. Rawat, S. Kaur, and P. Arun, “Study of the Damped Pendulum,” (2006), arXiv:physics/0608071 [physics].
- [84] J. Guo, *Journal of Hydraulic Research* **49**, 32 (2011).
- [85] S. R. Dahmen, (2014), 10.1140/epjh/e2015-50054-8, arXiv:1409.7446.
- [86] P. Klein, A. Müller, S. Gröber, A. Molz, and J. Kuhn, *American Journal of Physics* **85**, 30 (2017).
- [87] J. R. Graef, *Journal of Differential Equations* **12**, 34 (1972).
- [88] L. P. Fulcher, R. C. Scherer, A. Melnykov, V. Gateva, and M. E. Limes, *American Journal of Physics* **74**, 386 (2006).
- [89] R. Stoop, A. Kern, M. C. Göpfert, D. A. Smirnov, T. V. Dikanav, and B. P. Bezrucko, *European Biophysics Journal* **35**, 511 (2006).
- [90] A. Jenkins, *Physics Reports* **525**, 167 (2013).
- [91] Y. Kostov, R. Morshed, B. Höling, R. Chen, and P. B. Siegel, *American Journal of Physics* **76**, 956 (2008).
- [92] F. S. Crawford, *American Journal of Physics* **43**, 276 (1975).
- [93] B. Ravindra and A. Mallik, *Journal of Sound and Vibration* **170**, 325 (1994).
- [94] J. P. Baltanás, J. L. Trueba, and M. A. Sanjuán, *Physica D: Nonlinear Phenomena* **159**, 22 (2001).

- [95] R. Mickens, *Journal of Sound and Vibration* **264**, 1195 (2003).
- [96] S. J. Elliott, M. G. Tehrani, and R. S. Langley, *Philosophical Transactions of the Royal Society A: Mathematical, Physical and Engineering Sciences* **373**, 20140402 (2015).
- [97] A. R. Plastino, R. S. Wedemann, E. M. F. Curado, F. D. Nobre, and C. Tsallis, *Phys. Rev. E* **98**, 012129 (2018).
- [98] P. Flores, J. Ambrósio, J. P. Claro, and H. M. Lankarani, “Contact-impact force models for mechanical systems,” in *Kinematics and Dynamics of Multi-body Systems with Imperfect Joints: Models and Case Studies* (Springer Berlin Heidelberg, Berlin, Heidelberg, 2008) pp. 47–66.
- [99] O. Muvengi, J. Kihui, and B. Ikua, *Proceedings of Sustainable Research and Innovation Conference* **0**, 99 (2014).
- [100] P. J. Sebastião, *European Journal of Physics* **35**, 015017 (2013).
- [101] C. Grosse, *Journal of Colloid and Interface Science* **419**, 102 (2014).
- [102] N. Minorsky, *Journal of Applied Mechanics* **9**, 65 (1942).
- [103] G. Cerullo and S. De Silvestri, *Review of Scientific Instruments* **74**, 1 (2003).
- [104] Y. Shen, *Nonlinear Infrared Generation*, Topics in Applied Physics (Springer Berlin Heidelberg, 2006).
- [105] R. Boyd and D. Prato, *Nonlinear Optics* (Elsevier Science, 2008).
- [106] G. Lehmann, K. H. Spatschek, and G. Sewell, *Phys. Rev. E* **87**, 063107 (2013).
- [107] F. Schluck, G. Lehmann, and K. H. Spatschek, *Physics of Plasmas* **22**, 093104 (2015).
- [108] J. M. Christian, *European Journal of Physics* **38**, 055002 (2017).
- [109] S. M. George and C. B. Harris, *Phys. Rev. A* **28**, 863 (1983).
- [110] I. Boscolo, F. Castelli, M. Stellato, and S. Vercellati, arXiv e-prints, arXiv:1402.5318 (2014), arXiv:1402.5318 [physics.ed-ph].
- [111] A. B. Basset, *A treatise on hydrodynamics: with numerous examples*, Vol. 2 (Deighton, Bell and Company, 1888).
- [112] W. S. Hamilton, “Fluid force on accelerating bodies,” in *Coastal Engineering 1972*, pp. 1767–1782.
- [113] R. A. Heringe, *The Chemical Engineering Journal* **11**, 89 (1976).
- [114] P. J. Thomas and P. J. Thomasa, **2090** (1992), 10.1063/1.858379.
- [115] F. Mainardi, P. Pironi, and F. Tampieri, *Proceedings CANSAM* **95**, 836 (1995).
- [116] T.-J. Chang and B. C. Yen, *Journal of Engineering Mechanics* **124**, 1193 (1998).
- [117] F. Candelier, J. R. Angilella, and M. Souhar, *Physics of Fluids* **16**, 1765 (2004).
- [118] M. A. van Hinsberg, J. H. ten Thije Boonkamp, and H. J. Clercx, *Journal of Computational Physics* **230**, 1465 (2011), arXiv:1008.0833.
- [119] D. Baleanu, R. Garra, and I. Petras, *Reports on Mathematical Physics* **72**, 57 (2013).
- [120] A. Daitche, *Journal of Fluid Mechanics* **782**, 567 (2015), arXiv:1501.04770.
- [121] S. Annamalai and S. Balachandar, *Journal of Fluid Mechanics* **816**, 381 (2017).
- [122] H. J. Maris, *American Journal of Physics* **87**, 643 (2019).
- [123] F. Tatom, *Applied Scientific Research* **45**, 283 (1988).
- [124] F. Mainardi, “Fractional calculus. some basic problems in continuum and statistical mechanics,[in:] a. carpinteri, f. mainardi (eds.), *fractals and fractional calculus in continuum mechanics*,” (1997).
- [125] A. E. González, F. A. Bombardelli, and Y. I. Niño, *Journal of Hydraulic Engineering* **134**, 1513 (2008).
- [126] N. Lukerchenko, *Journal of Hydraulic Engineering* **136**, 853 (2010).
- [127] M. Du, Z. Wang, and H. Hu, *Scientific Reports* **3**, 1 (2013).
- [128] O. Özgen, *Physics-Based Animation Models Using Fractional Calculus*, Ph.D. thesis, UC Merced (2013).
- [129] P. Olejnik and J. Awrejcewicz, *Mechanical Systems and Signal Processing* **98**, 91 (2018).
- [130] S. Sakakibara, *JSME International Journal Series C* **40**, 393 (1997).
- [131] M. Seredyńska and A. Hanyga, *Acta Mechanica* **176**, 169 (2005).
- [132] C. Yin, F. Liu, and V. Anh, *Journal of Algorithms & Computational Technology* **1**, 427 (2007).
- [133] R. L. Bagley and P. J. Torvik, *Journal of Rheology* **27**, 201 (1983).
- [134] P. J. Torvik and R. L. Bagley, *Journal of Applied Mechanics* **51**, 294 (1984).
- [135] L. Gaul, P. Klein, and S. Kemple, *Mechanical Systems and Signal Processing* **5**, 81 (1991).
- [136] R. Metzler and T. F. Nonnenmacher, *International Journal of Plasticity* **19**, 941 (2003).
- [137] A. Aribi, C. Farges, M. Aoun, P. Melchior, S. Najar, and M. N. Abdelkrim, *Communications in Nonlinear Science and Numerical Simulation* **19**, 3679 (2014).
- [138] A. Falaize and T. Hélie, in *International Symposium on Musical Acoustics* (Le Mans, France, 2014) pp. 1–5, cote interne IRCAM: Falaize14d.
- [139] J. Quintana, A. Ramos, and I. Nuez, *IFAC Proceedings Volumes* **39**, 432 (2006), 2nd IFAC Workshop on Fractional Differentiation and its Applications.
- [140] R. L. Magin, *Computers and Mathematics with Applications* **59**, 1586 (2010).
- [141] F. Mainardi, *Mathematics* **6**, 4 (2018).
- [142] M. Li, *Symmetry* **10** (2018), 10.3390/sym10020040.
- [143] F. Odar and W. S. Hamilton, *Journal of Fluid Mechanics* **18**, 302 (1964).
- [144] G. D. Catalano, *AIAA Journal* **23**, 1627 (1985).
- [145] M. Parmar, A. Haselbacher, and S. Balachandar, *Journal of Fluid Mechanics* **699**, 352 (2012).
- [146] S. Lambertz, *Experimentelle Untersuchung der Basset Gedächtniskraft auf eine starre Kugel in instationärer Bewegung — Experimental measurement of the history forces on a rigid sphere in unsteady motion*, Ph.D. thesis.
- [147] M. Parmar, A. Haselbacher, and S. Balachandar, *Phys. Rev. Lett.* **106**, 084501 (2011).
- [148] C. J. Lawrence and S. Weinbaum, *Journal of Fluid Mechanics* **171**, 209–218 (1986).
- [149] M. Abbad and M. Souhar, *Experiments in Fluids* **36**, 775 (2004).
- [150] C. Coimbra, *Annalen der Physik* **12**, 692 (2003).
- [151] H. Pedro, J. Pereira, M. Kobayashi, and C. Coimbra, “History forces in oscillating convective flow past a fixed particle,” in *43rd AIAA Aerospace Sciences Meeting and Exhibit* (2005) p. 1393.

- [152] R. L. Bagley and P. J. Torvik, *Journal of Rheology* **27**, 201 (1983).
- [153] M. Moshrefi-Torbati and J. K. Hammond, *Journal of the Franklin Institute* **335**, 1077 (1998).
- [154] I. Podlubny, , 1 (2008), arXiv:0110241v1 [arXiv:math].
- [155] J. F. Gómez-Aguilar, R. F. Escobar-Jiménez, M. G. López-López, and V. M. Alvarado-Martínez, *European Physical Journal Plus* **133** (2018), 10.1140/epjp/i2018-11924-1.
- [156] A. Ebaid, *Applied Mathematical Modelling* **35**, 1231 (2011).
- [157] S. Rekhviashvili, A. Pskhu, P. Agarwal, and S. Jain, *Turkish Journal of Physics* **43**, 236 (2019).
- [158] S. Khubalkar, A. Junghare, M. Aware, and S. Das, *International Journal of Electrical Engineering Education* , 1 (2018).
- [159] H. Richard, *Fractional calculus: an introduction for physicists* (World Scientific, 2014).
- [160] M. D. Ortigueira and J. A. Tenreiro Machado, *Journal of Computational Physics* **293**, 4 (2015).
- [161] M. Seredyńska and A. Hanyga, *Journal of Mathematical Physics* **41**, 2135 (2000).
- [162] P. D. Spanos and G. I. Evangelatos, *Soil Dynamics and Earthquake Engineering* **30**, 811 (2010).
- [163] K. Diethelm, N. J. Ford, and A. D. Freed, *Nonlinear Dynamics* **29**, 3 (2002).
- [164] H. Gavin, “Numerical integration for structural dynamics,” <https://pdfs.semanticscholar.org/4907/eb47e4924ff9d32a643b8acc9dd0666c94c4.pdf> (2001).
- [165] N. Heymans and I. Podlubny, *Rheologica Acta* **45**, 765 (2006).
- [166] B. N. N. Achar, C. F. Lorenzo, and T. T. Hartley, “The caputo fractional derivative: Initialization issues relative to fractional differential equation,” in *Advances in Fractional Calculus: Theoretical Developments and Applications in Physics and Engineering*, edited by J. Sabatier, O. P. Agrawal, and J. A. T. Machado (Springer Netherlands, Dordrecht, 2007) pp. 27–42.
- [167] A. Gladkina, G. Shchedrin, U. A. Khawaja, and L. D. Carr, “Expansion of fractional derivatives in terms of an integer derivative series: physical and numerical applications,” (2017), arXiv:1710.06297 [math.NA].
- [168] D. Threlfall, *Mechanism and Machine Theory* **13**, 475 (1978).
- [169] W. H. Press, S. A. Teukolsky, W. T. Vetterling, and B. P. Flannery, *Numerical Recipes 3rd Edition: The Art of Scientific Computing*, 3rd ed. (Cambridge University Press, New York, NY, USA, 2007).
- [170] L. B. Magalas, *Journal de Physique IV Colloque* **6**, 17 (1996).